Balancing Robustness, Transparency and Superwetting via Embedding Functional Nanoparticles in V-Groove Architectures

Yi Xie[1], Hao Zhang[1], Xinran Li[1], Jian Luo[1], Xiong Qian[2*], Yong Zheng[2], Chuanlin Hu[1], Ivan P. Parkin[3], Lee Li[4], Zhi Chen[5], Xiujian Zhao[1]*

[1] State Key Laboratory of Silicate Materials for Architectures, Wuhan University of Technology, No. 122, Luoshi Road, Wuhan 430070, P. R. China.

[2] Department of Civil and Environment Engineering, and Research Centre for Resources Engineering towards Carbon Neutrality, The Hong Kong Polytechnic University, Hong Kong, China.

[3] Department of Chemistry, University College London, London WC1H 0AJ, U.K.

[4] State Key Laboratory of Advanced Electromagnetic Engineering and Technology (Huazhong University of Science & Technology), No.1037, Luoyu Road, Wuhan, P. R. China.

[5] Wuhan Shuneng New Material Co., LTD, Wuhan, P. R. China.

Abstract

The development of transparent and mechanically durable superamphiphobic (SAP) and superhydrophobic (SH) coatings remains challenging due to the inherent trade-offs between surface micro-nano architecture, optical clarity, liquid repellency, and mechanical resistance. Herein, we present a balancing strategy that combines femtosecond laser-etched V-groove microstructures on glass substrate with functionalized SiO_2 nanoparticles. This approach results in transparent and mechanically robust superwetting coatings with water and oil contact angles of 173.6° and 170.4°, respectively, while the average spectral transmittance ranging from 380 to 1100 nm can be enhanced from 80.4% in the uncoated laser-etched glass to 82.1% in the SAP coated etched glass. The laser-etched V-groove architecture serves as a structural confinement framework, enhancing nanoparticle adhesion and providing mechanical robustness, thereby maintaining stable SH performance even after 50 cycles of abrasion test. As a sharp comparison, the SAP coated non-etched sample loses its liquid repellency after 2 friction cycles. Furthermore, the SAP coated sample demonstrates excellent chemical and environmental stability, retaining superwetting properties under acidic, neutral, salt environments, and prolonged UV illumination. The proposed method not only addresses the challenge of balancing optical transparency with superwetting performance and mechanical robustness but also offers a practical route for fabricating multifunctional coatings with self-cleaning and anti-icing, suitable for applications in architectural glazing, photovoltaics, and optical protection systems.

Keywords

Laser etching; superamphiphobicity; superhydrophobicity; transparent coating; mechanical stability; anti-icing

1. Introduction

Transparent superhydrophobic (SH) and superamphiphobic (SAP) coatings (TSHCs) represent a cutting-edge innovation in materials science, combining optical clarity and liquid repellency to meet the demanding applications in various fields such as photovoltaics (PVs),[1-3] wearable devices,[4] automotive industry,[5-7] medical devices,[8] and architecture. [9] Driven by applications like lenses, windows, and PVs, the vast majority of research and performance reporting focuses on the visible spectrum (380-780 nm). In PV field, thanks to the self-cleaning performance, a transparent SH coating can prevent incident light loss and reduce degradation of PV conversion efficiency that results from dust deposition during prolonged operation.[10] For instance, by combination of spin-coating and spray deposition, the as-fabricated SH antireflective coatings displayed water contact angle (WCA) of 168° and water sliding angle (WSA) of 2°, respectively, enabling similar J-V characteristics and conversion efficiency to those of uncoated solar device. [11] The textured hot-embossed fluoropolymer film with low refraction and SH performance (WCA = 156 ± 1°, WSA = 8 ± 3°) facilitated to a reduction in surface contamination on PV modules, which consequently enhanced the generation of top cover photocurrent. [12] In a PV device covered by a SH transparent three-layer system with a WCA of 153° and transparency of 94%, the solar efficiency decreased to 14.81% in 60 days, which is lower than that of the bare solar cell (21% reduction in solar efficiency).[3]

Despite significant progress, the development of coatings that exhibit SH and SAP properties along with high optical transparency, mechanical durability, and environmental sustainability remains a technical challenge. For example, achieving high transparency inherently conflicts with superhydrophobicity. Superhydrophobicity relies on nano/micro-scale surface roughness to trap air (Cassie-Baxter state), while a roughness usually scatters light and reduces transparency. Many research reports demonstrated coatings with 85-92% average visible light transmittance while maintaining high WCAs (>150°) and low WSAs (<10°). The challenge lies in how to simultaneously realize mechanical properties, SH or SAP performances, and high transmittance through material design and structure optimization.[13]

Conventional strategies for the fabrication of TSHCs often involve a multistep sol-gel route,[14, 15] self-assembly process,[16] template-assisted spray coating method,[17, 18] chemical vapor deposition,[19, 20] hydrothermal method,[7] or ammonia-based hydrolysis systems.[21] Most of these

techniques pose either processing complexity or environmental concerns. In many cases, the optical transparency of the coating is sacrificed due to light scattering from disordered or oversized surface textures, while abrasion resistance is heavily limited by the weak mechanical adhesion of the functional layer to the substrate.[22] The trade-off between structural roughness (required for liquid droplet mobility) and optical clarity (required for visual or PV applications) has hindered the practical application of such coatings on transparent substrates, including glass.[18]

Micro-nano structured rough surfaces, which are critical to realize SH and SAP performance, are usually fragile and highly susceptible to abrasion. Many efforts such as combining paint and adhesives,[23] constructing multiscale particle system,[24] design of gradient and nacre-like structures,[25, 26] and microstructure design with protective framework armor,[27] have been explored to improve the robustness of SH surfaces. Particularly, embedding functionalized nanoparticles (NPs) or low-surface-energy molecules into mechanically stable protective armor has been verified to be an effective technique to achieve robust SH surfaces. Microstructures created by laser etching-assisted procedure enable us the fabrication of SH surfaces with enhanced mechanical durability, which has been realized by a post-treatment such as chemical modification in the presence of low-surface-energy molecules[28, 29] and filling the as-etched textures with functional NPs.[30, 31] Most of the previously reported laser etching-assisted fabrication of superwetting surfaces was obtained on non-transparent substrates such as metals and polymers,[32] which have shown potential in anti-corrosion, fog collection, and anti-icing.[28, 33, 34] However, glass substrate enabling transparent functional coatings, which would be more promising in the fields of PVs, anti-fogging, etc., was rarely reported in laser-etching for the fabrication of transparent SAP coatings.[35-37]

Motivated by the above-mentioned challenges and inspired by existing research, herein, we propose a strategy integrating alkaline-catalyzed surface functionalization of SiO_2 NPs with precision microstructural design for balancing robustness, transparency, and superwetting of TSHCs.[17, 38, 39] Instead of conventional ammonia catalysts, we employ NaOH as a benign alternative to promote the surface modification in the presence of hexamethyl disilazane (HMDS) or perfluorooctyltriethoxysilane (POTS) for SiO_2 NPs.[40] This is environmentally friendly and avoids uncontrolled hydrolysis, reduces particle agglomeration, and enables the formation of a porous but optically smooth coating layer.[41] Simultaneously, we introduce a femtosecond laser-

etched glass substrate with periodic V-groove topography, which acts as not only a microreservoir for embedding functional NPs but also structural shields against mechanical damage.[42]

The integration of NaOH-assisted surface functionalization of SiO_2 NPs with reentrant V-groove microstructures enables the fabrication of coatings with exceptional SAP and SH performances. The optimized SAP coating exhibits WCA and oil contact angle (OCA) of up to 173.6° and 170.4°, respectively. The average spectral transmittance of SAP coated etched glass ranging from 380 to 1100 nm can reach 82.1%, surpassing that of uncoated laser-etched glass (80.4%). More importantly, the coatings demonstrate remarkable durability, retaining their SAP performance even after more than 50 abrasion cycles—far exceeding the performance of non-structured systems. This durability is primarily attributed to the V-groove array's confinement effect, which effectively minimizes lateral particle loss during abrasion, coupled with the stable surface modification achieved through silanization. This work presents a scalable and environmentally friendly strategy for producing robust SAP and SH coatings with superior mechanical resilience and anti-reflection properties. By combining localized microstructural reinforcement with optimized surface chemistry, this work offers a versatile pathway for developing advanced interface materials suitable for optical protection, anti-contamination, and energy harvesting applications.[43]

2. Experimental Section

2.1. Materials

Ethanol (≥99.7%, analytical grade), tetraethyl orthosilicate (TEOS, AR) were purchased from Sinopharm Chemical Reagent Co. Ltd. Hexamethyl disilazane (HMDS, AR), NaOH (96.0%), fumed SiO_2 NPs (15 nm, 99.9%), acetone (99.0%) and perfluorooctyltriethoxysilane (POTS, $CF_3(CF_2)_7CH_2CH_2Si(OC_2H_5)_3$, ≥97%) were purchased from Aladdin. The glass substrates were cleaned by sequential ultrasonication in acetone, ethanol, and deionized (DI) water before use. All chemicals were used as received without any further purification.

2.2. Preparation and surface modification of SiO_2 NPs

All experiments were conducted at RT. Regarding the fabrication of SH coating, the SiO_2 NPs and the surface modification by methyl groups were realized following a previously reported procedure,[40] except that the NaOH concentration was 1.8 M and the HMDS amount was 1.0 mL.

Regarding the fabrication of SAP coating, 1.0 g of commercial fumed SiO_2 NPs was dispersed in 100 mL ethanol under magnetic stirring. Then, NaOH aqueous solution (0.7 mL, 1.8 M) and DI water (6 mL) were added to initiate a basic catalytic environment. After 30 min of stirring, 0.35 mL of POTS was introduced as the fluorosilane surface-modifying agent. The mixture was continuously stirred for 6 h to ensure sufficient surface modification and uniform dispersion. The obtained transparent fluoroalkylsilane-modified SiO_2 NP dispersion was used for the subsequent dip-coating samples.

2.3. Laser etching glass substrates

The glass substrates for deposition were fabricated using a femtosecond laser system (YLET3030UF) with a laser spot size of 8 μm, a wavelength of 343 nm, and a pulse width of less than 350 fs. The repetition frequency was set between 1 kHz and 2 kHz to generate micro/nanostructured surfaces. To achieve a well-defined surface morphology, the laser power and scanning speed were optimized at 6 W and 1000 mm/s, respectively. By controlling the repetition count and scan spacing, laser-etched glass substrates with precisely structured microgrooves were obtained.

2.4. Fabrication of SAP and SH coatings

The SAP and SH coatings were fabricated using the laser-etched glass slide with well-defined V-groove microstructures as substrates. The substrates were vertically immersed in the methyl groups-modified (for SH coating) and fluoroalkylsilane-modified (for SAP coating) SiO_2 NP dispersion for 60 s and then withdrawn at a constant speed. The substrates were dried in ambient air without thermal curing. This one-step dip-coating process enabled uniform deposition of functional SiO_2 NPs into the etched grooves, forming a transparent and durable SH or SAP layer.

2.5. Characterization

The surface morphology was observed using field emission scanning electron microscopy (FESEM, Hitachi S–4800, Japan). Surface chemical information was examined via Fourier transform infrared spectroscopy (FTIR, Nicolet 6700, USA) over the 4000–400 cm^{-1} range. UV–Vis–NIR transmittance spectra and specular reflectance were measured with an UV–Vis–NIR spectrophotometer (Shimadzu UV–3600) using air as the background.

Surface wettability was evaluated by the water contact angles (WCAs), oil contact angles (OCAs), water sliding angles (WSAs) and oil sliding angles (OSAs), which were measured on a contact angle goniometer (Theta Lite, Biolin Scientific) using a 5 μL water droplet or bean oil droplet at room temperature. Each value was averaged from at least three independent measurements at different locations on the same coating.

2.6. Environmental stability evaluation

Chemical corrosion resistance was assessed by directly immersing the freshly coated substrates in NaCl solution, DI, acidic and alkaline solutions with different pH values, respectively, for different durations. After soaking, the samples were thoroughly rinsed with DI water, dried, and then collected WCAs/OCAs and WSAs/OSAs of water droplets on the coating surface to evaluate wettability retention. UV resistance was evaluated under continuous exposure of the samples to an ultraviolet mercury lamp (UVA–340, 40W) at a distance of 20 cm.

2.7. Mechanical durability test

Sandpaper abrasion test: The abrasion resistance test was performed via linear friction cycles using 2000 mesh sandpaper under a 50 g normal load which was equal to a pressure of 4.9 kPa. The sample was slid over a 10 cm distance per cycle at a constant speed of 2 cm/s, and contact/sliding angles were recorded after every 10 cycles for SAP/SH coated laser-etched glass and every 1 cycle for coated non-etched glass to assess performance retention.

Sand impact test: The impact resistance of the coating surface under dynamic conditions was evaluated by free falling ISO standard silica sand grains with 0.5–1.0 mm in size from a height of 10 cm above the coating onto the surface. The coating was secured to a support stand and inclined at 30°. To monitor the evolution of the surface wettability, WCAs/OCAs and WSAs/OSAs of the coating surface were recorded after each fall of a fixed volume of sand impacting the surface, followed by rinsing to remove the adhering sand and drying at RT.

Water impact test: Regarding the test of water droplet impact resistance, the coated glass slides were fixed at a 30^{o} tilt angle, and water droplets were continuously dripped from a height of 50 cm above the surface. Each droplet had a volume of 100 μL and the impact rate was 120 drops/min (i.e., 12 g/min). The WCAs/OCAs and WSAs/OSAs were measured after each fall of 400 g water.

2.8. Anti-icing test

The anti-icing experiments were conducted on a home-made setup, as described in our recent work.[44] Briefly, water droplets (50 μL) dyed by methylene blue (MB) were placed on sample surfaces, which were in a low-temperature chamber (e.g., -20 ºC). The entire freezing process of MB-dyed water droplets was monitored by a macro camera, and the freezing time was recorded to evaluate the anti-icing performance of different samples.

3. Results and Discussions

3.1. Design of superwetting coating on laser-etched microstructured glass

The design concept of the microstructured coating system is schematically illustrated in Figure 1a. The coating is fabricated by combining femtosecond laser-etched glass substrates with dip-coating of functional SiO_2 NPs. The laser etching process creates periodic inverted trapezoidal grooves with microstructure, providing mechanical confinement and physical anchoring for the embedded functional NPs. This structural framework significantly enhances coating adhesion and abrasion resistance. Typically, the transparent SAP coating was achieved through the deposition of SiO_2 NPs, which were fluorinated using perfluorooctyltrichlorosilane (POTS) assisted by NaOH instead of traditional ammonia catalysts.[45] This environmentally friendly process ensures stable surface modification and high optical clarity. As demonstrated in Figure 1 b–c, the coated SAP glass maintains clear, undistorted visual quality, with no perceptible difference between coated and uncoated regions under ambient lighting.

To validate the multifunctionality of the microstructured coating, we compared laser-etched and non-etched glass substrates before and after deposition of functional SiO_2 NPs. Upon immersing the substrates in the fluoroalkylsilane-modified SiO_2 NPs dispersion, the SAP micro-nano structure was successfully formed. The droplets of various simulated aqueous pollutants (e.g., coca cola, orange juice, green tea, coconut water, and MB solution) and various oils (e.g., bean oil, sesame oil, corn oil, pump oil, and n-hexadecane) of different surface tensions exhibited sphere-like shapes on the coated surfaces (Figure 1d–e), while they spread on the uncoated glass slides (Figure S1a and S1c of the Supporting Information (SI)), demonstrating excellent liquid repellency of the coated samples. Typically, the SAP coated laser-etched sample can achieve WCA and OCA up to 173.6° and 170.4°, respectively, and SAP coated non-etched sample exhibits WCA and OCA of 168.4° and 165.7°, respectively (see Figure S1b and S1d). Furthermore, the WSA and OSA of

all the coated samples remained below 10°, confirming a low adhesion regime and a stable Cassie–Baxter wetting state.

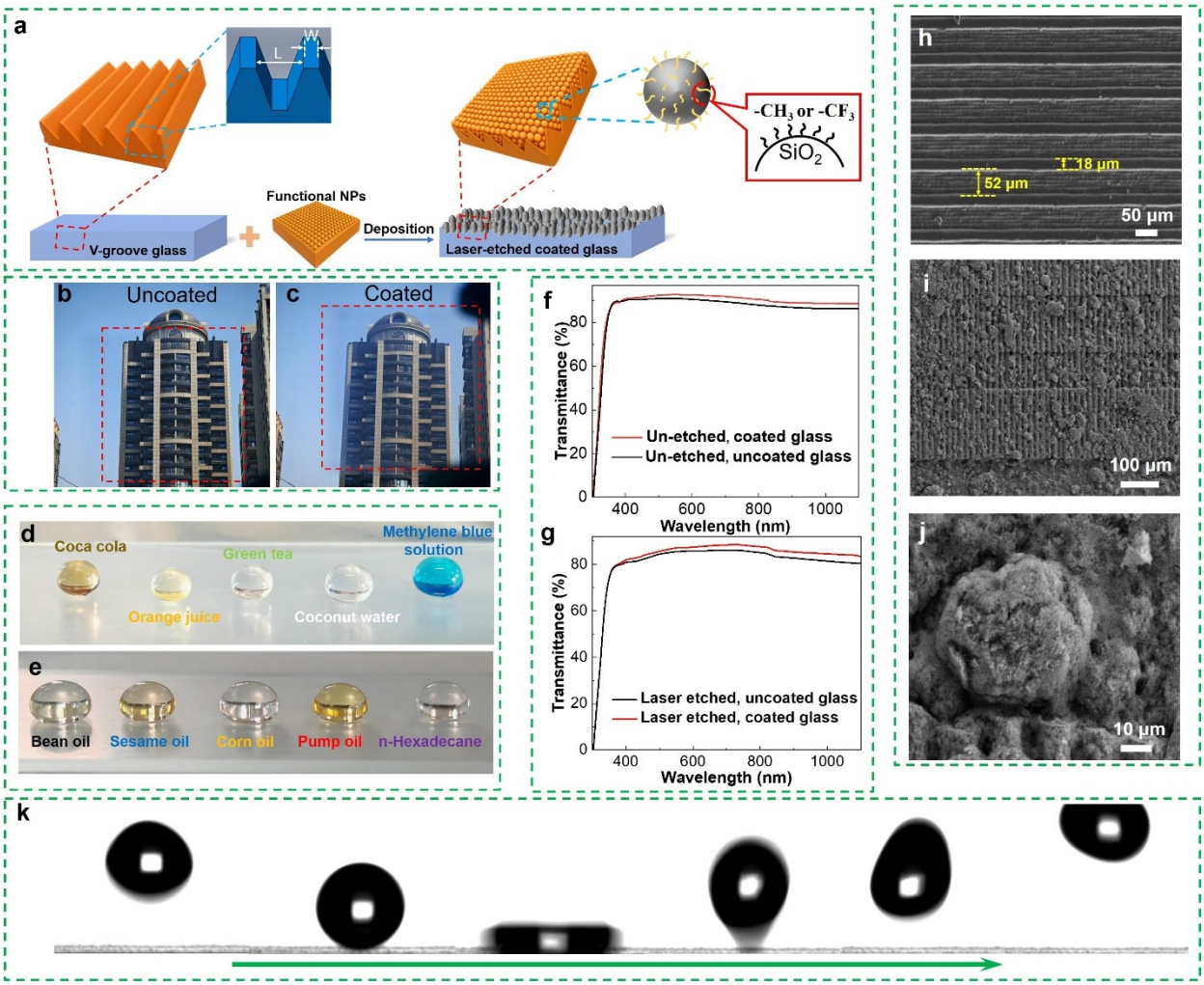

Figure 1. Design concept and fundamental performance of the laser-etched glass coating system. **(**a) Schematic of the laser-etched microstructure of the glass surface and fabrication of SAP and SH coatings composed of functional NPs-embedded V-grooves. (b–c) Photographic demonstration of the transparency of the laser-etched glass before (b) and after (c) coating. (d–e) Photos demonstrating various water-based droplets (d) and oil droplets (e) on SAP coated glass, respectively. (f–g) Optical transmittance spectra of non-etched glass and SAP coated non-etched glass (f), laser-etched glass and coated laser-etched glass (g). (h) SEM image of the uncoated laser-etched sample. (i–j) Low- and high-magnification SEM images of the representative SAP coated laser-etched sample. (k) Selected time-dependent pictures showing the water droplet (5.0 μL in volume) impacting and rebounding on SAP coated laser-etched sample.

Transparency of superwetting coatings is of great importance for practical application in PVs, anti-fogging, etc. We measured the optical transmittance spectra of the coatings and took photographs of the sample covering pictures, leaves or buildings to assess the transparency of the coatings. The transmittance spectra indicate that coatings deposited on both laser-etched and non-etched glass slides offer the samples anti-reflection performance compared with the uncoated glass slides (Figure 1f–g). As compared between the two black curves of Figure 1f–g, laser etching reduces the transmittance from 85.7% (across 300–1100 nm) in the uncoated non-etched glass slide to 80.4% after etching. The coated non-etched glass exhibits an average transmittance of 87.9% across 380–1100 nm, 2.2% higher than that of uncoated non-etched one (Figure 1f). Similarly, the SAP coated laser-etched glass slide demonstrates improvement (i.e., 1.7%) in transmittance (82.1%) compared to the uncoated etched state (80.4%), likely due to surface scattering reduction and refractive index matching from the nanoparticle layer.[46] Indeed, the comparison of the reflectance spectra shows that the SAP coated sample has lower reflectivity than the uncoated glass slide (Figure S2 of the SI), explaining the enhanced anti-reflection performance and spectral transmittance upon depositing SAP layer. The excellent spectral transmittance combined with pronounced water and oil repellency confirms the compatibility of the coating with optical and non-wetting functions in our work.

Surface morphology observations via SEM images (Figure 1h–j) confirm the functional advantage of the etched substrate. Before coating, the laser-etched glass surface displays well-defined parallel microgrooves with a 70 μm period, corresponding to the horizontal spacing between vertical scan lines (Figure 1h). This can be confirmed by analysis of the magnified SEM images (Figure S3a of the SI), which display rough-sided V-groove-shaped microgrooves with valleys and ridges.[36] The width of the protrusions (labeled as W, see also Figure 1a) and the width of V-grooves (labeled as L) are around 18 μm and 52 μm, respectively. After coating, SiO_2 NPs are densely and uniformly embedded within the grooves, forming a micro–nano structure (Figure 1i–j, Figure S3b of SI) that enhances liquid repellency and provides strong physical interlocking for improving mechanical durability. By contrast, non-etched coated samples show a relatively loose and non-uniform surface morphology (Figure S4 in the SI), with fewer anchoring sites, explaining their poor durability under mechanical stress, which will be discussed later in the following sections.

Figure 1k reports the selected snapshots of a 5.0 μL water droplet impacting on the SAP coated laser-etched glass slide. Upon impact with the SAP surface, the water droplet spreads into a pancake shape, contracts inward, and then fully rebound, indicating the presence of a Cassie-Baxter state of the coating and an intact air cushion formed by the hierarchical structure and low surface energy.

3.2. Laser-etched V-shaped microstructure enables enhanced mechanical robustness and functional retention

The laser-etched framework significantly enhances the mechanical robustness and functional retention of the coating system. This section establishes the structural and functional basis of our coating system and supports further investigations into its abrasion resistance and environmental robustness.[47] Figures 2a and 2b illustrate the fundamental differences in frictional response between the laser-etched SAP coating and the non-etched SAP coating. In the laser-etched system, functional SiO_2 NPs are embedded within groove valleys, providing mechanical confinement that prevents rapid loss of surface functionality during abrasion (Figure 2a). In contrast, non-etched coated surfaces lack structural anchoring, resulting in extensive nanoparticle detachment even upon weak friction, leading to a rapid decline in liquid repellent performance (Figure 2b). Various tests such as sandpaper friction resistance, water droplet impact, falling sand impact, and tape peeling were conducted to support the enhanced mechanical robustness by embedding the functional nanoparticles in laser-etched V-groove-shaped microstructure, which will be discussed in the following sections.

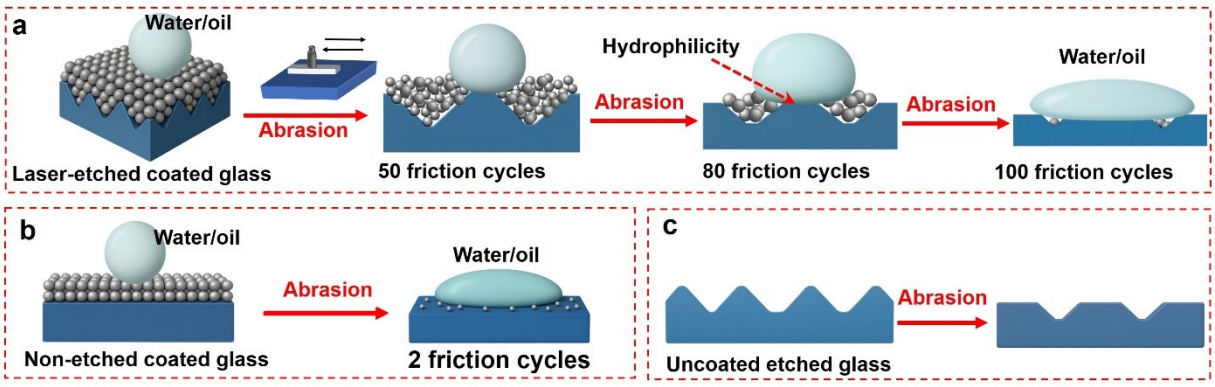

Figure 2. Schematic illustrating the mechanism of the enhanced mechanical stability of SAP laser-etched glass with embedded functional NPs. (a) Friction mechanism schematic of SAP

laser-etched glass with embedded functional NPs. (b) Friction mechanism schematic of SAP coated non-etched glass. (c) Friction mechanism schematic of uncoated laser-etched glass without embedded NPs.

To elucidate the wear resistance mechanism of the laser-etched SAP coating, experiments of morphological and wettability evolution over controlled sandpaper friction cycles were conducted.[48, 49] As shown in Figure 3a and 3b, the wetting performance of laser-etched samples remains stable, with the WCA exceeding 150° and 125° after 50 and 70 friction cycles, respectively. After 10 cycles, the surface maintains superoleophobic performance (OCA around 156°), though oleophobicity decreases more after 20 cycles of abrasion (OCA below 134°). In stark contrast, the non-etched coated SAP sample loses its SAP performance within 2 cycles, with the WCA rapidly dropping to 134.0° and the WSA increasing to 16.9°. After only one cycle of abrasion, the OCA plummets to 66.0° and OSA increases to 79.2°, primarily due to the lack of structural support and early particle detachment.

The transmittance spectra (Figure 3c) show that the laser-etched coated glass retains an average transmittance of 75.7% (from 380 to 1100 nm) even after 50 cycles of abrasion test, and slightly decreases to 74.1% after 100 abrasion cycles. Real-object transparency and surface wetting performance tests further support these findings. As illustrated in insets of Figure 3c, after 50 and 10 friction cycles, respectively, the MB-dyed water droplets and bean oil droplets on the coated laser-etched glass maintain a sphere-like shape with high mobility, demonstrating the sustained superhydrophobic and superoleophobic performance after mechanical abrasion. In contrast, the non-etched coated glass loses its amphiphobicity and shows significantly reduced liquid droplet mobility after 2 cycles of the abrasion test due to insufficient microstructural support and rapid detachment of functional SiO_2 NPs.

SEM images captured after friction cycles reveal the morphological evolution (Figure 3d and 3e). Initially, the laser-etched surface coated with SiO_2 NPs exhibits a uniform and compact NP layer filling the etched cavities. After 50 friction cycles, the groove width (i.e., L) decreases from approximately 52 μm to 40 μm, and the width of superhydrophilic protrusion (i.e., W) increases from 18 μm to 30 μm (Figure 3d, Figure S5a–b of the SI), indicating moderate wear but retained structure. At this point, the sample surface preserves rough micro-nanostructure within the laser-etched area (Figure 3d, Figure S5c in the SI), facilitating the liquid repellency of the surface. At

100 cycles, the groove width further reduces to 25 μm, and the protrusion width widens to 45 μm (Figure 3e), indicating the significant collapse of the protective microstructure and loss of capacity for retaining functional NPs (Figure S5d–f of the SI), and explaining the substantial reduction in liquid repellency.

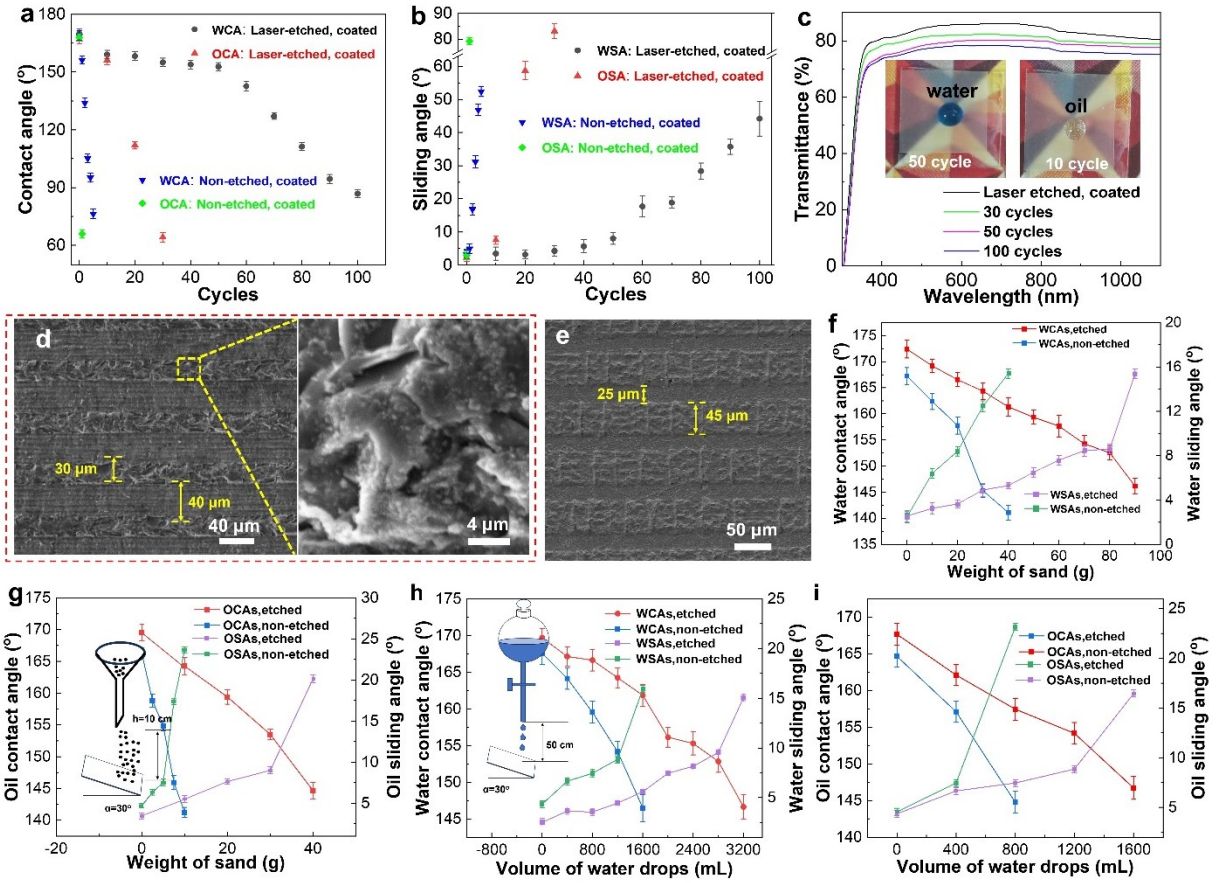

Figure 3. Mechanical resistance of the SAP coated laser-etched and non-etched coated samples. (a) Contact angle (WCA, OCA) vs. friction cycles for SAP laser-etched and non-etched coated glass. (b) Sliding angle (WSA, OSA) vs. friction cycles for SAP laser-etched and non-etched coated glass. (c) Optical transmittance spectra of the samples after different friction cycles for SAP coated laser-etched glass slides. Insets display the transparency demonstration, water and bean oil droplets states of coated laser-etched glass after 50 cycle and 10 cycle of friction test, respectively. (d–e) SEM images of SAP coated laser-etched after 50 (d) and 100 (e) friction cycles, respectively. (f–g) Evolution of WCAs, WSAs (f), OCAs and OSAs (g) upon falling sand impacting on SAP coated laser-etched and SAP coated non-etched samples, respectively.

(h–i) Evolution of WCAs, WSAs (h), OCAs and OSAs (i) upon water droplet impacting on SAP coated laser-etched and SAP coated non-etched samples, respectively. Inset in panel h provides the schematic illustration of the test set up.

As a general recipe to demonstrate the improved mechanical durability while keeping the high transparency by protective V-groove-shaped microstructure, SH coating was also fabricated by dip-coating the laser-etched glass slide into functional SiO_2 dispersion. In this case, the SiO_2 NPs were pre-modified by methyl groups in the presence of HMDS. The SEM images, optical transmittance spectra, initial surface wettability, and water droplet bouncing performance of the typical SH coated etched samples are reported in Figures S6 and S7 of the SI. Clearly, compared to the uncoated laser-etched glass slide, the as-coated laser-etched sample displays anti-reflection property and excellent water repellent performances. Figure S8 and S9 of the SI further report the evolution of WCAs, WSAs and surface morphology over abrasion cycles. The surface maintains its superhydrophobicity with WCA and WSA of 151° and 10°, respectively, even after 60 cycles of abrasion test (Figure S8a of the SI). For comparison, the coated non-etched glass surface has lost its superhydrophobicity even after experiencing abrasion for only 1 cycle (Figure S8b of the SI). Upon repeated friction cycles, the surface morphology undergoes progressive changes. The sublayer of SiO_2 NPs was exposed upon friction and a new micro-nano hierarchical structure was formed. The groove width (W) gradually decreases from 52 μm to 46 μm after 50 cycles of abrasion test, and finally to 42 μm after 100 cycles (Figure S9 of the SI). Meanwhile, the width of the superhydrophilic protrusions (L) increases from 18 μm to 24 μm and then to 28 μm due to abrasion-induced structural fatigue. Nevertheless, SiO_2 NPs remain densely packed within the groove interiors, especially after 50 abrasion cycles, indicating that the etched cavities effectively retain the particles under mechanical stress. These embedded NPs maintain a hierarchical structure capable of trapping air, thereby preserving the surface's liquid-repellent functionality. However, as confirmed by SEM images, extended abrasion reveals smoothing of the nanoparticle layer on the V-shaped-groove ridges and progressive collapse of the sidewalls, which reduces groove depth and destroys the re-entrant geometry. This structural degradation along with exposure of intrinsic superhydrophobic non-etched areas leads to an increase in true solid–liquid contact and triggers a Cassie–to–Wenzel transition, reducing water and oil contact angles and causing the degeneration of SH and SAP performances.

For further comparison, Table S3 of the SI provides the summarization of the wear resistance for various transparent SH surfaces,[18, 50] where the L_w is the maximum wear distance without losing SH performance. In our case the coating sustains 5000 mm at 4.9 kPa with 2000-grit, which indicates a competitive—often stronger—abrasion tolerance under a more demanding regime. Some representative previously-reported entries include: 5000 mm at 1.63 kPa (electrodeposition; 1000-grit); 2000 mm at 3.9 kPa (laser + anodizing; 600-grit); at the low-pressure extreme, 1000 mm at 0.26 kPa (template-spray; 2000-grit). Clearly, our laser-etched, NPs-embedded architecture preserves superhydrophobicity over *Lw*=5000 mm at 4.9 kPa, i.e., at one of the highest pressures among the surveyed transparent systems, suggesting that the present SAP and SH coatings have promising potential in practical engineering. It is noteworthy that the mechanical durability of the coated sample is mainly dependent on the mechanical resistance of the microstructure of the uncoated laser-etched glass substrate, specifically, the mechanical strength of the protrusions. This conclusion can be confirmed by the direct observation of SEM images collected on the uncoated laser-etched glass surface after 50 and 100 cycles of abrasion test (Figure S10 of the SI; see again the schematic illustration in Figure 2c). Indeed, the groove width (W) decreases from 52 μm to 41 μm and finally to 36 μm after 50 and 100 cycles of abrasion test, respectively (Figure S10 of the SI). These observations indicate that the mechanical robustness can be further enhanced by optimizing not only groove microstructure but also the hardness and strength of the substrate.

Sand impact test, water droplet impact resistance and tape peeling test were further conducted to evaluate the enhanced mechanical robustness of the SAP surface via laser-etched microstructure (Figure 3f–i, Figure S11 of the SI). The CAs and SAs as function of sand exposure for SAP coated laser-etched and SAP coated non-etched samples were monitored to assess the evolution of surface wettability during falling sand.[51] The WCA of the SAP coated laser-etched sample gradually decreased from 173.6° to 151.6° after 80 g of sand impact, and the OCA remained to be 152.9° after 30 g of sand impact (Figure 3f–g, red curves), meanwhile the WSAs and OSAs are smaller than 10°. These results indicate the preservation of the liquid repellency. In sharp contrast to that of SAP coated laser-etched sample, the SAP coated non-etched sample had lost its superhydrophobicity and superoleophobicity after 30 g and 7.5 g of sand impact, respectively (Figure 3f–g, blue curves). These observations indicate that the effective protection of functional NPs by etched V-shaped microstructure against sand impact.

The water droplet impact resistance of the SAP coated non-etched and etched coatings was evaluated. [52] As illustrated by the inset of Figure 3h, the coating was secured to a support stand and inclined at 30°, and water was continuously dropped from a height of 50 cm (see the detailed procedure in the Experimental section). The variations of WCAs, WSAs, OCAs and OSAs were recorded during continuous water droplet impact (Figure 3h–i). It was noticed that the SAP coating can retain its SH property even after the impact of 2800 g droplets; the WCAs decreased from initial 173.6º to 151.8º and WSAs were still smaller than 10º. However, WCA decreased to 148.1º after water drop impact of 1200 g, while the WSA increased 132º at this point, indicating the loss of the SH performance. Similar comparison of OCAs and OSAs between the SAP etched and non-etched samples is reported in Figure 3i, confirming the enhanced mechanical stability of the SAP coated etched sample upon water droplet impact. All these results undoubtedly verify that laser-etched structural anchoring is essential to preserve superamphiphobicity under mechanical abrasion and impact, collectively validating the functional mechanism proposed in Figure 2a.

Tape peeling test was further performed to compare the adhesion ability of the SAP coating to glass substrates with and without laser etching. Herein, considering the unique V-shaped microstructure, a high-tack tape is directly pressed firmly onto the coating surface without pre-cutting like we did before,[26] and then it is peeled off vertically to monitor the evolution of surface wettability over cycles of tape peeling. It was noticed that the SAP surface without laser etching has lost its SAP functionality even after 1–2 cycles of peel-off test (not shown here). By contrast, though the WCAs and OCAs gradually decreased as the peel-off cycles increased, WCA and OCA can be preserved to be above 150º after 12 and 4 cycles of test, respectively (Figure S11 of the SI). As an example, WCA declined to 151.1° and WSA increased to 9.3° after 12 cycles of test. This comparison highlights the enhanced mechanical robustness of the SAP coating by embedding functional NPs to laser-etched microstructure.

3.3. Chemical and environmental durability

To further evaluate the practical durability of the SAP coated etched sample under complex environmental conditions, the long-term chemical resistance and ultraviolet (UV) stability are systematically assessed by monitoring the evolution of surface wettability over time when exposed to acidic/basic/salt environment and UV irradiation (Figure 4, and Figure S12 of the SI).[52-54] The coated glass was immersed in deionized water, sodium chloride (3.5 wt%), and solutions with

different pH values adjusted by tuning dilute hydrochloric acid and sodium hydroxide solutions, for 40 days. The coating surface was rinsed with DI water and dried, followed by tracking of the surface wetting behavior. The WCAs remain to be 161.1°, 154.7° and 155.1° (Figure 4a) after 40 days of soaking in DI water, NaCl solution, and acidic environments, respectively. Meanwhile, the WSAs can be preserved below 10^o (not shown here) throughout the testing period. Similar results can be noticed for the evolution of OCAs and OSAs on the SAP surface under the above environments (Figure 4b), indicating robust resistance to hydrolytic and acidic attack. However, in alkaline solution, the WCA declined markedly below 150^o after 36 hours (Figure S12a of the SI), reflecting the breakdown of surface nanostructure and loss of superhydrophobicity. The loss of liquid repellency in an alkaline environment is attributed to the alkali-induced dissolution of the SiO_2 framework and hydrolysis of the siloxane bonding network, which together lead to a significant reduction in surface roughness. As shown in Figure 4c, the tested coatings before and after soaking in acidic solution for 40 days retained a transmittance level above 85.2% across the 380 – 1100 nm range, ensuring their viability for transparent applications. The photographic insets embedded in Figure 4c display that both water and bean oil droplets are in sphere-like shape, which further validates the preservation of SAP performance over extended chemical exposure in acidic environment.

Further, the coating's performance under continuous UV irradiation was evaluated over 40 days. As depicted in Figure 4d, the WCA and OCA can remain essentially unchanged, with only a minor increase in sliding angle, confirming the excellent photostability of the fluorinated SiO_2 network. The stability under UV illumination is largely attributed to the chemical inertness of the perfluorinated groups and the dense particle distribution that shields the underlying substrate from UV-induced oxidation or hydrolysis. The practical optical clarity before and after UV irradiation is also visually confirmed by the insets of Figure 4d, where images of natural surfaces (leaves) remain sharp and color-accurate. This visual clarity, coupled with the verified long-term resistance to water, acid, and UV irradiation, affirms that the present SAP coating system, realized by combination of laser-etching with embedding functional NPs can offer a rare balance of superamphiphobicity, durability, and high transparency, which is difficult to achieve in traditional systems.

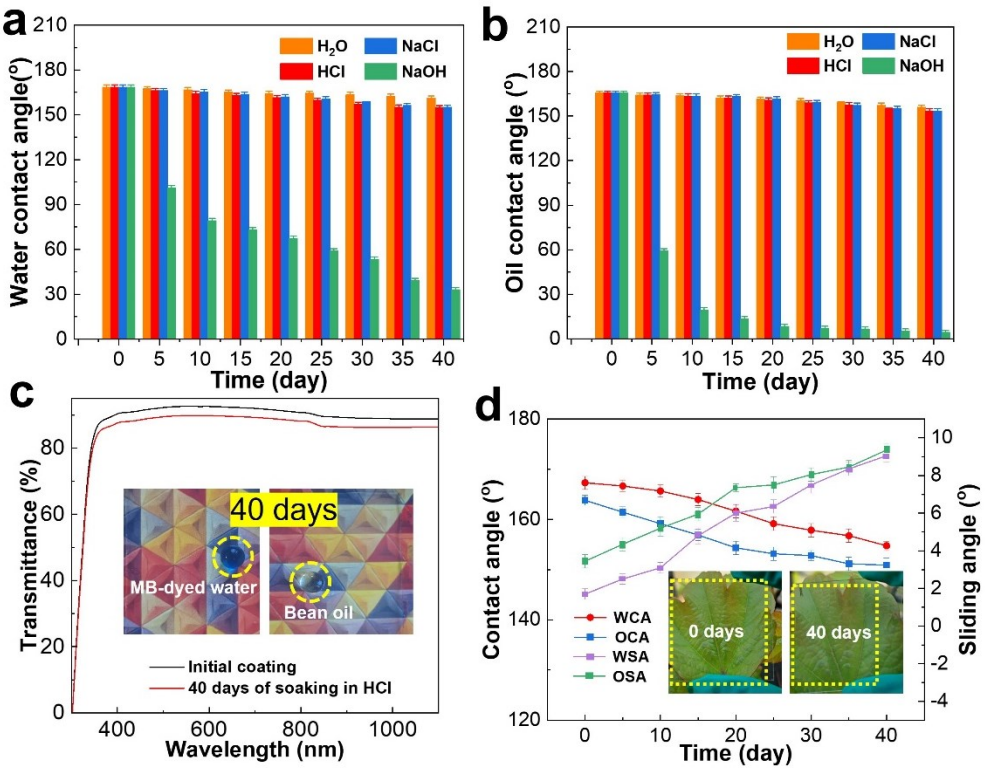

Figure 4. Environmental stability of the representative SAP coated laser-etched glass sample. (a–b) Time-dependent OCAs (a) and WCAs (b) under immersion in H_2O, HCl, NaCl, and NaOH solutions, respectively. (c) Transmittance spectra of the SAP coated laser-etched glass before and after soaking in HCl solution for 40 days. Insets provide the digital photographs of the SAP sample together MB-dyed water and bean oil droplets on the surface. (d) Time-dependent WCAs, OCAs, WSAs and OSAs under UV irradiation. Insets provide the photographic demonstration of transparency of the coated laser-etched glass before and after UV irradiation for 40 days.

In summary, the SAP and SH coated laser-etched samples exhibit significantly improved mechanical robustness and environmental durability in comparison with the non-etched samples. This comprehensive design strategy underscores the importance of synergistically optimizing structure, surface energy, and formulation parameters to meet the rigorous demands of real-world transparent protective surfaces. In this unique system, the laser-etched grooves act as microscale particle traps, mechanically interlocking functional NPs while maintaining a rough surface of micro-nano structure for air entrapment (Cassie–Baxter state). The gradual loss of performance under abrasion is consistent with morphological degradation, where once the groove geometry collapses below a critical threshold, the Cassie–Baxter state transfers toward a Wenzel-type

wetting regime. Upon sandpaper abrasion, the width of the V-groove and protrusion progressively change, compromising surface integrity and wetting resistance.[50, 55] With continued abrasion, the collapse of the micro–nano structure and increased exposure of superhydrophilic protrusions lead to a gradual loss of surface liquid repellency. The observed trends in both contact angle retention and microstructural degradation confirm the design logic and highlight the importance of optimizing the surface microgeometry and chemical environment.[56]

3.4. Self-cleaning and Anti-icing performance

Self-cleaning and anti-icing performance of TSHCs are of great importance in practical applications in PVs, automotive industry, etc. In fact, because the Cassie–Baxter state that yields superamphiphobicity also reduces solid–liquid contact and heat transfer, the same surface inherently resists ice nucleation. The following anti-icing test therefore serves to illustrate a secondary manifestation of the superamphiphobic interface rather than a distinct application. In our work, the previously discussed water droplet impacting and rebounding performance (see again Figure 1k and Figure S7d of the SI) suggest the presence of a Cassie-Baxter state, which facilitates self-cleaning of the SAP and SH coatings. As further confirmed in Videos S1 and S2 of the SI, the low sliding angle enables not only water but also oil droplets to easily roll off (Videos S1 and S2 of the SI), highlighting the surface's potential for anti-contamination applications. As shown in Video S1, the SAP surface was stained by hydrophilic fly-ash powder, followed by casting water droplets on the surface to investigate the self-cleaning performance. Rolling droplets effectively remove contaminants along their path, making the surface clean (see also Figure S13 and Video S3 of the SI). In contrast, droplets adhere to the uncoated hydrophilic glass, retaining surface fouling (Figure S14 of the SI). These results demonstrate the self-cleaning and antifouling capabilities of the transparent SAP-coated laser-etched glass slides.

Anti-icing strategies of SH coatings typically involve repelling incoming droplets before freezing, delaying ice formation, lowering the ice nucleation temperature,[57, 58] and reducing ice–surface adhesion after freezing.[59, 60] In our work, the anti-icing performance of the coating was evaluated by recording the freezing delay time of water droplets in a simulated cold environment (relative humidity = 60%).[44, 61] The MB-dyed water droplets (50 μL) were cast on the various surfaces to be tested, then the freezing process of the water droplets was monitored (Figure 5, Figure S15–S17 of the SI). As the icing process proceeds progressively from the bottom to the top

of the water droplet, icing delay time was recorded at the point when a peach-tip-like shape of ice is formed.[62]

As noticed from Figure 5, overall, the freezing time of the MB-dyed water droplets on all samples decreases as the environmental temperature decreased from -10 ºC to -20 ºC. Besides, at a specified temperature, the freezing time of water droplets on laser-etched glass slide is slightly shorter than that on non-etched glass slide. For example, at -20 ºC, the water droplets completely froze after 65 seconds on uncoated laser-etched glass, while the freezing time was slightly extended to 80 seconds on non-etched glass (Figure 5a, Figure S17a–b of the SI). The shorter freezing time on the laser-etched glass is attributed to the intrinsic superhydrophilicity of the uncoated surface and the V-groove microstructure, which increases the contact area between the droplet and the cooling substrate.

Noticeably, compared to the rapid icing of water droplets on uncoated glass, the SAP and SH coatings exhibited significantly prolonged freezing time. As demonstrated in Figure 5a–b, the freezing time of water droplets has been significantly delayed to 280 seconds and 400 seconds at -20 ºC on the SH and SAP coated laser-etched glasses (see also Figure S17e–f of the SI), respectively, suggesting a significantly enhanced anti-icing performance via deposition of non-wetting functional NPs. At the same temperature (i.e., -20 ºC), the corresponding SH and SAP coatings formed on non-etched glass slides exhibit relatively shorter freezing times of 220 and 310 seconds, respectively (Figure S17b–c of the SI). Similar evolution can be noticed at other temperatures such as -10 ºC and -15 ºC (Figure S15 and S16 of the SI). For instance, the freezing time of the water droplets on SH and SAP coated laser-etched glass slides can reach up to 330 and 435 seconds, respectively. Overall, the substantial improvement of anti-icing performance of coated laser-etched glass is primarily attributed to the thermal insulating SiO_2 NPs, the existence of "air cushion" at the solid-water interface and the reduced contact area between solid and water due to the hierarchical micro-nanostructure and large WCA.[63] The SAP coating exhibits the highest WCA, resulting in minimal solid–water contact. This effectively limits heat transfer from water droplet to the substrate and significantly delays icing.[64] Receding contact area indicates less probability of heterogeneous ice nucleation, slowing down ice formation.

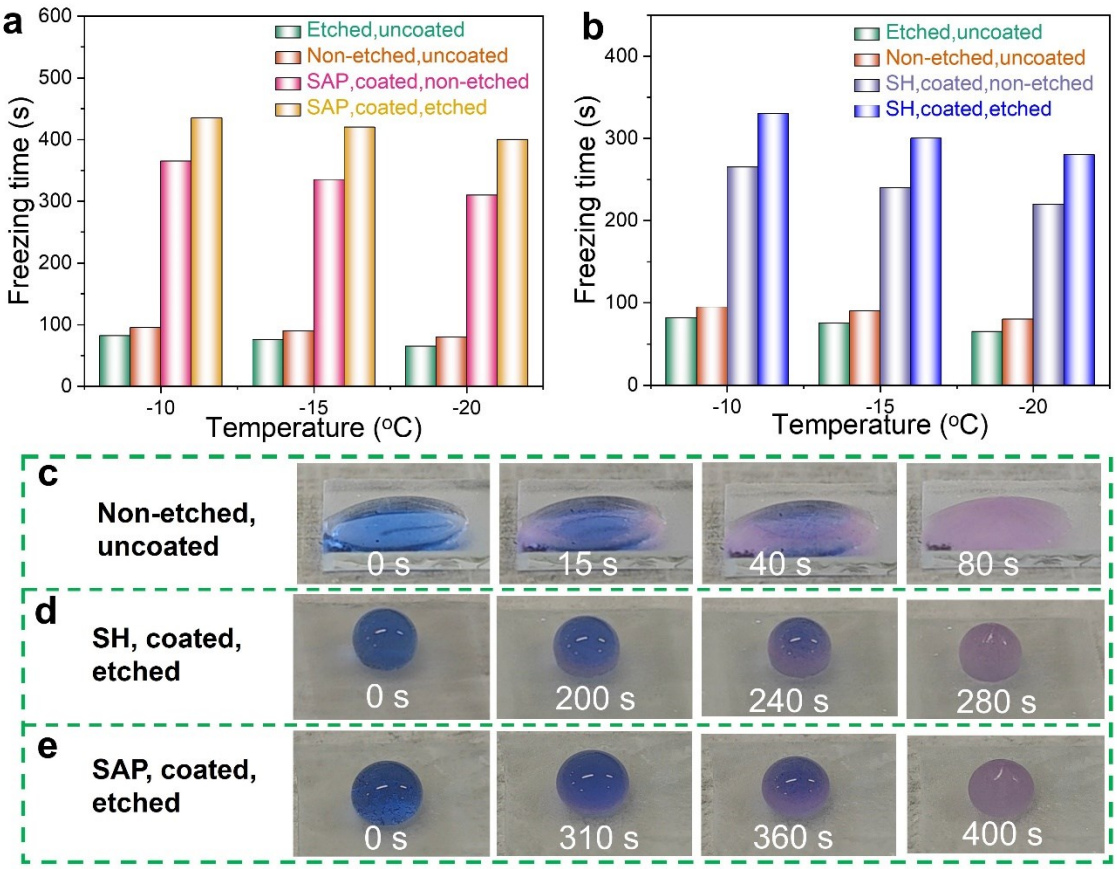

Figure 5. Anti-icing properties of the various representative coatings. (a) Freezing time for the SAP coatings at different temperatures. (b) Freezing time for the SH coatings at different temperature under 1.0 sun illumination. For comparison, the freezing time for uncoated glass slides is provided. (c–e) Digital photographs during water droplet freezing on uncoated laser-etched glass (c), SH coated laser-etched glass (d), and SAP coated laser-etched glass (e), respectively, demonstrating the freezing time at -20 °C.

3.5. Mechanism on balancing liquid repellency, transparency, and durability

The construction of SAP or SH and anti-reflection coatings in this study relies on a finely balanced combination of surface chemical modification, hierarchical roughness generation, and controlled NP packing. To elucidate how the coating simultaneously achieves optical transparency, liquid super-repellency, and mechanical/chemical stability, we optimized the synthesis parameters by systematically investigating the impact of POTS dosage, NaOH amount, and SiO_2 NPs content on the surface wetting performance and transparency of the coated non-etched glass slides. As

shown in Figure 6a–b, both the WCAs and OCAs vary with POTS concentration, reaching a maximum of 168.4° and 165.7°, respectively, at an optimal POTS dosage of 0.35 mL. At low POTS addition dosage (< 0.2 mL), the surface coverage by fluorinated groups is incomplete, resulting in reduced WCA and OCA and high sliding resistance. With increasing POTS amount, both WCA and OCA rise sharply, reaching maxima around 0.35 mL, where the low-surface-energy modification is sufficient to stabilize a Cassie–Baxter state. However, a further increase in POTS content leads to deterioration of wetting performance. This is due to excess silane aggregation and partial pore filling, which smoothens the surface, decreases the effective roughness, and impairs air retention beneath liquid droplets. Correspondingly, Figure 6c shows a decline in optical transmittance when POTS exceeds optimal levels, confirming that excessive silane impairs both non-wetting property and optical clarity.

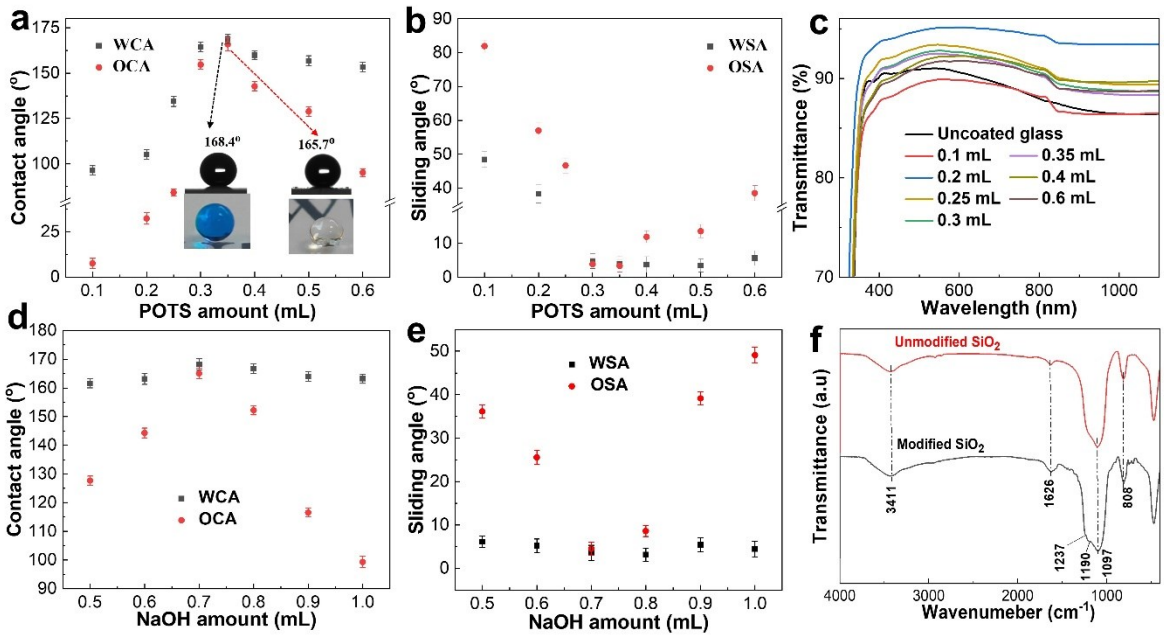

Figure 6. Influence of POTS and NaOH dosage on contact angle, sliding angle, optical transmittance, and FTIR of the coated glass. (a–b) WCAs/OCAs (a) and WSAs/OSAs (b) as a function of POTS concentration. (c) Optical transmittance spectra of coatings achieved with different POTS contents. (d–e) WCAs/OCAs (d) and WSAs/OSAs (e) as a function of NaOH amounts. (f) FTIR spectra before and after SiO_2 particle modification.

We emphasized that the surface functioning of SiO_2 NPs in our case was realized with the assistance of NaOH, making the procedure environmentally friendly. The influence of NaOH

amount (in volume) on the surface wettability and transparency was explored in fabrication of transparent SH coatings. [40] Herein, the evolution of WCAs/OCAs and spectral transmittance spectra is depicted in Figure 6d–e, and Figures S18–S19 of the SI. Relative to the uncoated glass slide, NaOH amount more than 0.1 mL enabled an anti-reflection property of the resulting SAP coated glass (Figure S19 of the SI). Moderate NaOH (0.5–0.7 mL) facilitates the realization of superamphiphobicity, and either too little or too much NaOH impairs surface performance (Figure 6d–e): insufficient catalysis yields poor chemical modification, while excess NaOH densifies the particle network or even dissolves the SiO_2 structure, leading to loss of roughness and SAP performances.

FTIR analysis (Figure 6f) confirms the successful surface modification of SiO_2 NPs after NaOH-assisted fluorosilane treatment. The peaks at the wavenumbers of 3411 cm^{-1} and 1626 cm^{-1} were assigned to the stretching and bending vibrations of hydroxyl groups (–OH), respectively.[65] The characteristic vibrations that appeared at 1097 cm^{-1} and 808 cm^{-1} correspond to the stretching Si–O–Si group.[20] Compared with the unmodified sample, new peaks appear at 1237 cm^{-1} and 1109 cm^{-1} after surface modification in the presence of POTS, corresponding to the asymmetric vibrations of $–CF_2–$ and $–CF_3$ stretching,[20] indicating successful fluorination. This transformation enables the as-modified NPs to display SAP performance after embedding in the V-groove microstructure.

Overall, the exceptional transparency, liquid repellency and durability of the TSHCs arise from the cooperative action of the laser-etched V-shaped-groove architecture and the functionalized SiO_2 nanoparticle layer. The re-entrant micro-scale V-shaped grooves and hierarchical nano-texture trap a stable air cushion, sustaining a Cassie–Baxter state that minimizes the real solid–liquid contact and produces high WCAs and OCAs. At the same time, the sub-wavelength packing of the SiO_2 nanoparticles creates a gradual refractive-index transition, leading to the enhanced spectra transparency compared with the uncoated glass slides. Furthermore, the grooves act as a mechanical cradle that anchors the nanoparticle network and redistributes shear stress, explaining the outstanding abrasion and chemical resistance. The mechanical strength of the substrates for laser-etching, dimensions of the etched and non-etched area, compositional tuning and surface modification effectively adjust the balance of micro-nano structure, surface wettability, spectral transparency and durability of the coating.

4. Conclusion

We developed a transparent SAP and SH coating strategy by integrating femtosecond laser-etched microgrooves with embedding functional SiO_2 NPs. The designed groove geometry provides structural confinement and mechanical interlocking, enabling both high visible-light transmittance and robust liquid repellency. By optimization of the POTS and NaOH dosages, the representative as-fabricated SAP coated laser-etched sample achieves superamphiphobicity with WCAs and OCAs exceeding 170° and spectral transmittance was increased by 2.2% relative to the uncoated etched glass slide. Unlike conventional sol–gel methods, the NaOH-assisted surface fluorination leverages direct silane condensation on fumed SiO_2 NPs under alkaline catalysis, ensuring uniform coverage without unwanted hydrolysis. The scalable fabrication process is performed at RT and suitable for diverse substrates, offering potential applications in self-cleaning optical interfaces, transparent protection layers, and multifunctional coatings for architectural, photovoltaic, and anti-fouling technologies.

The durability of the coating under abrasion is attributed to the synergistic effects of groove retention, capillary shielding, and stable molecular grafting, maintaining visual clarity even after extensive friction cycles. Additionally, the coating exhibits not only an outstanding anti-icing property but also strong chemical and environmental stability against acids, UV exposure, and prolonged immersion.

Declaration of Competing Interest

The authors declare that they have no known competing financial interests or personal relationships that could have appeared to influence the work reported in this paper.

Data availability

Data will be made available on request.

Acknowledgments

This work is supported by National Natural Science Foundation of China (No. U24B2094).

Appendix A. Supplementary Data

Supplementary data including digital photographs of samples, SEM images, WCAs/WSAs, OCAs/OSAs, water/oil repellency and self-cleaning demonstrations, transmittance spectra, anti-icing performance, and videos of droplet dynamics to this article can be found online.

References

1. S. S. Ingole; R. S. Sutar; P. P. Gaikwad; A. R. Jundle; R. A. Ekunde; S. H. Liu; S. S. Latthe, "A Review on Transparent Superhydrophobic Coatings for Self-Cleaning Solar Cell Panels: Its Fabrication, Robustness and Industrial Implementation," *Surfaces and Interfaces* **2025,** 70.https://doi.org/10.1016/j.surfin.2025.106794
2. M. S. Mozumder; A. H. I. Mourad; H. Pervez; R. Surkatti, "Recent Developments in Multifunctional Coatings for Solar Panel Applications: A Review," *Solar Energy Materials and Solar Cells* **2019,** 189, 75-102.https://doi.org/10.1016/j.solmat.2018.09.015
3. Z. Liang; Z. Zhou; L. Zhao; B. Dong; S. Wang, "Fabrication of Transparent, Durable and Self-Cleaning Superhydrophobic Coatings for Solar Cells," *New Journal of Chemistry* **2020,** 44 (34), 14481-14489.https://doi.org/10.1039/d0nj01402h
4. B. N. Sahoo; J. Woo; H. Algadi; J. Lee; T. Lee, "Superhydrophobic, Transparent, and Stretchable 3D Hierarchical Wrinkled Film-Based Sensors for Wearable Applications," *Advanced Materials Technologies* **2019,** 4 (10), 11.https://doi.org/10.1002/admt.201900230
5. B. Nomeir; S. Lakhouil; S. Boukheir; M. A. Ali; S. Naamane, "Durable and Transparent Superhydrophobic Coating with Temperature-Controlled Multi-Scale Roughness for Self-Cleaning and Anti-Icing Applications," *Progress in Organic Coatings* **2024,** 189.https://doi.org/10.1016/j.porgcoat.2024.108338
6. A. M. S. Seukep; D. R. Pandzou; Z. X. Cui; D. Kuzhandaivel; L. Kinkpe; X. Zhou; Z. X. Weng; L. H. Zheng; J. L. Wang; X. H. Ding; L. X. Wu, "Robust, Transparent, and Superhydrophobic PVDF-TrFE/PDMS Nanofiber Coatings for Anti-Fogging and Anti-Icing," *Progress in Organic Coatings* **2025,** 208.https://doi.org/10.1016/j.porgcoat.2025.109470
7. M. J. Reshma; J. Jiya; M. Anshida; J. Amala; P. Shajesh; S. Anas, "A Two-Tier Synthetic Marvel for Developing Antibacterial, Self-Cleaning, Durable, Transparent, and Superhydrophobic Surfaces Using Zinc Oxide - Methyltrimethoxysilane Hybrids," *Journal of Environmental Chemical Engineering* **2024,** 12 (2), 11.https://doi.org/10.1016/j.jece.2024.112007
8. A. Mirza; A. Mishra; A. Rajput; A. Ali; R. Goswami, "Nanostructured Transparent Superhydrophobic Coating for Glass and Plastic: Study of Antimicrobial Characteristics," *Materials Today Communications* **2025,** 42.https://doi.org/10.1016/j.mtcomm.2024.111419
9. W. Y. Liu; L. Y. Zhuang; J. J. Liu; Y. Liu; L. L. Wang; Y. He; G. Yang; F. Shen; X. H. Zhang; Y. Z. Zhang, "Make the Building Walls Always Clean: A Durable and Anti-Bioadhesive Diatomaceous Aarth@SiO_2 Coating," *Construction and Building Materials* **2021,** 301, 8.https://doi.org/10.1016/j.conbuildmat.2021.124293
10. R. A. Sathya; C. Ponraj, "Superhydrophobic Route of Fabricating Antireflective, Self-Cleaning, and Durable Coatings for Solar Cell Applications," *Journal of Coatings Technology and Research* **2024,** 21 (1), 1-30.https://doi.org/10.1007/s11998-023-00843-x
11. I. Torun; N. Celik; M. Hancer; F. Es; C. Emir; R. Turan; M. S. Onses, "Water Impact Resistant and Antireflective Superhydrophobic Surfaces Fabricated by Spray Coating of

Nanoparticles: Interface Engineering via End-Grafted Polymers," *Macromolecules* **2018,** 51 (23), 10011-10020.https://doi.org/10.1021/acs.macromol.8b01808
12. A. Roslizar; S. Dottermusch; F. Vüllers; M. N. Kavalenka; M. Guttmann; M. Schneider; U. W. Paetzold; H. Hölscher; B. S. Richards; E. Klampaftis, "Self-Cleaning Performance of Superhydrophobic Hot-Embossed Fluoropolymer Films for Photovoltaic Modules," *Solar Energy Materials and Solar Cells* **2019,** 189, 188-196.https://doi.org/10.1016/j.solmat.2018.09.017
13. S. N. Ke; J. N. Li; R. D. Li; J. B. Zhu; Y. Chen; J. Hu; Y. K. Lai; J. Y. Huang; X. H. Wu; Z. Chen, "Recent Developments in the Fabrication, Performance, and Application of Transparent Superhydrophobic Coatings," *Advances in Colloid and Interface Science* **2025,** 342, 30.https://doi.org/10.1016/j.cis.2025.103537
14. S. S. Latthe; C. Terashima; K. Nakata; M. Sakai; A. Fujishima, "Development of Sol–Gel Processed Semi-Transparent and Self-Cleaning Superhydrophobic Coatings," *Journal of Materials Chemistry A* **2014,** 2 (15), 5548-5553.https://doi.org/10.1039/C3TA15017H
15. R. R. Hashjin; Z. Ranjbar; H. Yari; G. Momen, "Tuning up Sol-Gel Process to Achieve Highly Durable Superhydrophobic Coating," *Surfaces and Interfaces* **2022,** 33, 13.https://doi.org/10.1016/j.surfin.2022.102282
16. J. J. Lyu; B. R. Wu; N. Wu; C. Y. Peng; J. Yang; Y. Y. Meng; S. L. Xing, "Green Preparation of Transparent Superhydrophobic Coatings with Persistent Dynamic Impact Resistance for Outdoor Applications," *Chemical Engineering Journal* **2021,** 404.https://doi.org/10.1016/j.cej.2020.126456
17. H. Li; S. H. Tu; H. Y. Tu; M. Chen; S. X. Zhou; L. M. Wu, "Construction of Transparent, Robust and Haze-Selectable Superhydrophobic Coatings with Honeycomb Structure," *Chemical Engineering Journal* **2024,** 483, 149319.https://doi.org/10.1016/j.cej.2024.149319
18. H. J. Li; Q. Q. Jin; H. B. Li; H. Tong; K. K. Wang; S. R. Chen; G. F. Ouyang; Z. K. Wang; Y. A. Li, "Transparent Superamphiphobic Material Formed by Hierarchical Nano Re-Entrant Structure," *Advanced Functional Materials* **2024,** 34 (3), 2309684.https://doi.org/10.1002/adfm.202309684
19. X. C. Huang; M. Sun; X. Shi; J. L. Shao; M. H. Jin; W. N. Liu; R. H. Zhang; S. W. Huang; Y. M. Ye, "Chemical Vapor Deposition of Transparent Superhydrophobic Anti-Icing Coatings with Tailored Polymer Nanoarray Architecture," *Chemical Engineering Journal* **2023,** 454, 139981.https://doi.org/10.1016/j.cej.2022.139981
20. J. Lin; J. Du; S. Xie; F. Yu; S. Fang; Z. Yan; X. Lin; D. Zou; M. Xie; W. Ye, "Durable Superhydrophobic Polyvinylidene Fluoride Membranes via Facile Spray-Coating for Effective Membrane Distillation," *Desalination* **2022,** 538, 115925.https://doi.org/10.1016/j.desal.2022.115925
21. C. G. Li; G. H. Chang; S. L. Wu; T. Yang; B. J. Zhou; J. X. Tang; L. Z. Liu; R. Z. Guan; G. J. Zhang; J. Wang; Y. Yang, "Highly Transparent, Superhydrophobic, and Durable Silica/Resin Self-Cleaning Coatings for Photovoltaic Panels," *Colloids and Surfaces A: Physicochemical and Engineering Aspects* **2024,** 693, 133983.https://doi.org/10.1016/j.colsurfa.2024.133983
22. F. Z. Chen; Y. Q. Wang; Y. L. Tian; D. W. Zhang; J. L. Song; C. R. Crick; C. J. Carmalt; I. P. Parkin; Y. Lu, "Robust and Durable Liquid-Repellent Surfaces," *Chemical Society Reviews* **2022,** 51 (20), 8476-8583.https://doi.org/10.1039/d0cs01033b

23. Y. Lu; S. Sathasivam; J. Song; C. R. Crick; C. J. Carmalt; I. P. Parkin, "Robust Self-Cleaning Surfaces that Function when Exposed to either Air or Oil," *Science* **2015,** 347 (6226), 1132-1135.https://doi.org/10.1126/science.aaa0946
24. C. Hu; W. Chen; T. Li; Y. Ding; H. Yang; S. Zhao; E. A. Tsiwah; X. Zhao; Y. Xie, "Constructing Non-Fluorinated Porous Superhydrophobic SiO_2-Based Films with Robust Mechanical Properties," *Colloids and Surfaces A: Physicochemical and Engineering Aspects* **2018,** 551, 65-73.https://doi.org/10.1016/j.colsurfa.2018.04.059
25. Y. Xie; W. Xiong; S. Kareem; C. Qiu; Y. Hu; I. P. Parkin; S. Wang; H. Wang; J. Chen; L. Li; Z. Chen; H. Sun; X. Zhao, "Robust Superamphiphobic Coatings with Gradient and Hierarchical Architecture and Excellent Anti-Flashover Performances," *Nano Research* **2022,** 15 (8), 7565-7576.https://doi.org/10.1007/s12274-022-4386-3
26. T. H. Deng; L. S. Geng; H. L. Zhang; R. B. Ding; X. Qian; L. Li; T. Xu; W. H. Wu; Z. Chen; J. W. Chen; Y. Xie, "Resolving the Liquid Repellency-Mechanical Durability Trade-off via a Biomimetic Nacre-like Superamphiphobic Architecture," *Chemical Engineering Journal* **2025,** 520, 11.https://doi.org/10.1016/j.cej.2025.166032
27. D. H. Wang; Q. Q. Sun; M. J. Hokkanen; C. L. Zhang; F. Y. Lin; Q. Liu; S. P. Zhu; T. F. Zhou; Q. Chang; B. He; Q. Zhou; L. Q. Chen; Z. K. Wang; R. H. A. Ras; X. Deng, "Design of Robust Superhydrophobic Surfaces," *Nature* **2020,** 582 (7810), 55-59.https://doi.org/10.1038/s41586-020-2331-8
28. Y. Liu; H. Wang; Z. Zhang; H. Zhu; J. Song; C. Guo; C. Sun; K. Xu; J. Wang, "Laser-Chemical Composite Manufacturing of Biomimetic Stepped Armor Functional Metal Surface with Wear Resistance and Anti-Icing Characteristics," *Journal of Colloid and Interface Science* **2025,** 685, 49-62.https://doi.org/10.1016/j.jcis.2025.01.113
29. X. Zhang; L. Yang; T. Cui; X. Li; H. Wei, "Preparation of Stainless Steel Superhydrophobic Surface and Analysis of Hydrophobic Mechanism," *Langmuir* **2024,** 40 (39), 20715-20724.https://doi.org/10.1021/acs.langmuir.4c02801
30. X. Jiang; C. Zhou; J. Su; S. Tang, "Enhanced Anti-Icing Performance of Novel Superhydrophobic F-L@KH-SiO_2/OTMS Coating Synergistic Preparation with Bionic Micro-Nano Structures and Modified Nanoparticles," *Chemical Engineering Journal* **2024,** 498, 155264.https://doi.org/10.1016/j.cej.2024.155264
31. W. Shen; Z. Zhang; K. Xu; H. Zhu; Y. Liu; Y. Wu; S. Yang, "Reproducible PDMS Flexible Superhydrophobic Films: a Method Utilizing Picosecond Laser-Etched Templates," *Progress in Organic Coatings* **2024,** 189, 108344.https://doi.org/10.1016/j.porgcoat.2024.108344
32. Y. Guo; H. Zhao; G. Zhao, "Laser-Induced Superhydrophobic Polymer Surface for Droplet Manipulation, Controllable Light-Driven Actuator, and Underwater Motion Monitoring," *ACS Applied Materials & Interfaces* **2025,** 17 (8), 12707-12719.https://doi.org/10.1021/acsami.4c22766
33. G. Wang; J. Wang; K. Cheng; K. Yang; W. Zhang, "Nano Hierarchical Hill-Like Structure with TA1 Surface Manufactured by LIPSS for Anti-Corrosion and Anti-Icing," *Journal of Materials Research and Technology* **2025,** 35, 3655-3667.https://doi.org/10.1016/j.jmrt.2025.02.075
34. X. Li; G. Zhang; K. Du; S. Yin; Y. Liu; X. Xu; Y. Liu, "Fog Collection on Wettability-Mixed Patterned Surfaces Inspired by Multiple Biological Structures," *Chemical Engineering Journal* **2024,** 497, 154728.https://doi.org/10.1016/j.cej.2024.154728

35. L. B. Boinovich; E. B. Modin; A. R. Sayfutdinova; K. A. Emelyanenko; A. L. Vasiliev; A. M. Emelyanenko, "Combination of Functional Nanoengineering and Nanosecond Laser Texturing for Design of Superhydrophobic Aluminum Alloy with Exceptional Mechanical and Chemical Properties," *ACS Nano* **2017,** 11 (10), 10113-10123.https://doi.org/10.1021/acsnano.7b04634
36. B. Wang; Y. Q. Hua; Y. X. Ye; R. F. Chen; Z. B. Li, "Transparent Superhydrophobic Solar Glass Prepared by Fabricating Groove-Shaped Arrays on the Surface," *Applied Surface Science* **2017,** 426, 957-964.https://doi.org/10.1016/j.apsusc.2017.07.169
37. Y. Lin; J. P. Han; M. Y. Cai; W. J. Liu; X. Luo; H. J. Zhang; M. L. Zhong, "Durable and Robust Transparent Superhydrophobic Glass Surfaces Fabricated by a Femtosecond Laser with Exceptional Water Repellency and Thermostability," *Journal of Materials Chemistry A* **2018,** 6 (19), 9049-9056.https://doi.org/10.1039/c8ta01965g
38. W. X. Luo; J. F. Xu; G. Li; G. Q. Niu; K. W. Ng; F. Wang; M. J. Li, "Fabrication of Robust, Anti-Reflective, Transparent Superhydrophobic Coatings with a Micropatterned Multilayer Structure," *Langmuir* **2022,** 38 (23), 7129-7136.https://doi.org/10.1021/acs.langmuir.2c00264
39. R. Pan; H. J. Zhang; M. L. Zhong, "Triple-Scale Superhydrophobic Surface with Excellent Anti-Icing and Icephobic Performance via Ultrafast Laser Hybrid Fabrication," *ACS Applied Materials & Interfaces* **2021,** 13 (1), 1743-1753.https://doi.org/10.1021/acsami.0c16259
40. K. Shefiu; X. Yi; L. Tan; D. Yanxi; E. A. Tsiwah; A. S. A. Ahmed; J. W. Chen; F. Qiao; Z. Chen; X. J. Zhao, "Base-Catalyzed Synthesis of Superhydrophobic and Antireflective Films for Enhanced Photoelectronic Applications," *Journal of Materials Research and Technology* **2020,** 9 (3), 3958-3966.https://doi.org/10.1016/j.jmrt.2020.02.022
41. W. X. Zhang; J. Gao; Y. J. Deng; L. F. Peng; P. Y. Yi; X. M. Lai; Z. Q. Lin, "Tunable Superhydrophobicity from 3D Hierarchically Nano-Wrinkled Micro-Pyramidal Architectures," *Advanced Functional Materials* **2021,** 31 (24), 2101068.https://doi.org/10.1002/adfm.202101068
42. Y. Guo; H. B. Zhao, "Femtosecond Laser Processed Superhydrophobic Surface," *Journal of Manufacturing Processes* **2024,** 109, 250-287.https://doi.org/10.1016/j.jmapro.2023.12.005
43. H. Li; Z. H. Wang; H. Y. Tu; M. Chen; Y. Wu; L. M. Wu, "Leaf Vein-Inspired Transparent Superhydrophobic Coatings with High Stability," *Science China-Materials* **2025,** 68 (4), 1203-1211.https://doi.org/10.1007/s40843-024-3269-6
44. H. Zhang; C. Qiu; R. Zhang; H. Zhang; Y. Chen; T. Zeng; F. Qiao; L. Li; G. Ali; X. Zhao; Y. Xie, "Superwetting MAX@SiO_2 Coatings with High Photothermal Conversion Performances for Efficient Seawater Desalination and Anti-/De-Icing," *Chemical Engineering Journal* **2024,** 496, 153707.https://doi.org/10.1016/j.cej.2024.153707
45. P. Zhu; L. J. Zhu; F. F. Ge; G. Wang; Z. X. Zeng, "Robust and Transparent Superamphiphobic Coating Prepared via Layer-by-Layer Spraying," *Surface & Coatings Technology* **2021,** 426, 127793.https://doi.org/10.1016/j.surfcoat.2021.127793
46. X. Deng; L. Mammen; H. J. Butt; D. Vollmer, "Candle Soot as a Template for a Transparent Robust Superamphiphobic Coating," *Science* **2012,** 335 (6064), 67-70.https://doi.org/10.1126/science.1207115
47. C. R. Yu; A. Shanmugasundaram; D. W. Lee, "Nanosilica Coated Polydimethylsiloxane Mushroom Structure: a Next Generation Flexible, Transparent, and

Mechanically Durable Superhydrophobic Thin Film," *Applied Surface Science* **2022,** 583, 152500.https://doi.org/10.1016/j.apsusc.2022.152500
48. K. Liao; W. J. Wang; X. S. Mei; W. Q. Zhao; H. Yuan; M. Q. Wang; B. Z. Wang, "Stable and Drag-Reducing Superhydrophobic Silica Glass Microchannel Prepared by Femtosecond Laser Processing: Design, Fabrication, and Properties," *Materials & Design* **2023,** 225, 111501.https://doi.org/10.1016/j.matdes.2022.111501
49. J. Kim; K. H. Oh, "Evaluation of the Cross-Sectional Shape of μ-Grooves Produced in Stainless Steel 304 by Laser-Induced Etching Technique," *Micromachines* **2021,** 12 (2), 14.https://doi.org/10.3390/mi12020144
50. A. B. Gurav; H. Shi; M. Duan; X. Pang; X. Li, "Highly Transparent, Hot Water and Scratch Resistant, Lubricant-Infused Slippery Surfaces Developed from a Mechanically-Weak Superhydrophobic Coating," *Chemical Engineering Journal* **2021,** 416, 127809.https://doi.org/10.1016/j.cej.2020.127809
51. G. Polizos; G. G. Jang; D. B. Smith; F. A. List; M. G. Lassiter; J. Park; P. G. Datskos, "Transparent Superhydrophobic Surfaces Using a Spray Coating Process," *Solar Energy Materials and Solar Cells* **2018,** 176, 405-410.https://doi.org/10.1016/j.solmat.2017.10.029
52. B. Nomeir; S. Lakhouil; S. Boukheir; N. Abdallah; S. Naamane; M. A. Ali, "Synthesis of a Novel High-Performance Siloxene Based 2D Material for Durable and Transparent Superhydrophobic Coatings with Self-Cleaning and Anti-Icing Properties," *Industrial & Engineering Chemistry Research* **2025,** 64 (12), 6460-6474.https://doi.org/10.1021/acs.iecr.4c04098
53. M. Boutamart; S. Rafqah; A. Hadri; K. Nouneh; S. Zaidi; H. Bichara; S. Briche, "Design of Fluorine-Free Superhydrophobic Coating for Fibred Architectonic Concrete," *Construction and Building Materials* **2024,** 425, 11.https://doi.org/10.1016/j.conbuildmat.2024.136086
54. T. P. Rasitha; N. G. Krishna; B. Anandkumar; S. C. Vanithakumari; J. Philip, "A Comprehensive Review on Anticorrosive/Antifouling Superhydrophobic Coatings: Fabrication, Assessment, Applications, Challenges and Future Perspectives," *Advances in Colloid and Interface Science* **2024,** 324, 41.https://doi.org/10.1016/j.cis.2024.103090
55. Z. Chen; Z. Yang; Z. Zhang; J. Li; G. Zhang; F. Han, "A New Preparation Method of Hierarchical Microstructure for Wear-Resistant Superhydrophobic Surface," *Journal of Materials Research and Technology* **2025,** 36, 4134-4146. https://doi.org/10.1016/j.jmrt.2025.04.132
56. P. Y. Zhang; Z. G. Guo, "Multienergy Barrier Anti-/Deicing Surface with Excellent Photothermal Effect," *ACS Applied Materials & Interfaces* **2025,** 17 (6), 9680-9689.https://doi.org/10.1021/acsami.4c19263
57. R. Pradhan; H. S. Grewal, "Towards Sustainability: An Eco-Friendly Approach for Durable Anti-Icing Superhydrophobic Surfaces," *Small Methods* **2024,** 8 (12), 2400459.https://doi.org/10.1002/smtd.202400459
58. Y. D. Zhang; Z. G. Guo, "Lobelia-Inspired Photothermal Storage Flexible Film for Efficient Deicing," *Small Methods* **2025,** 9 (7), 2402006.https://doi.org/10.1002/smtd.202402006
59. Y. Z. Li; A. M. Sha; Z. Tian; Y. S. Cao; X. Z. Li; Z. Z. Liu, "Review on Superhydrophobic Anti-Icing Coating for Pavement," *Journal of Materials Science & Technology* **2023,** 58 (8), 3377-3400.https://doi.org/10.1007/s10853-023-08212-0

60. Q. Li; Z. G. Guo, "Fundamentals of Icing and Common Strategies for Designing Biomimetic Anti-Icing Surfaces," *Journal of Materials Chemistry A* **2018,** 6 (28), 13549-13581.https://doi.org/10.1039/c8ta03259a
61. R. Zhang; H. Zhang; Y. Zhong; S. Tian; X. Qian; L. Li; J. S. Shayeh; R. Sedghi; X. Zhao; Y. Xie, "Photothermal CuS@SiO_2 Nanocomposites for Solar-Driven Anti-Icing/Deicing and Synchronous Evaporation and Photocatalysis," *Journal of Materials Chemistry A* **2025,** 13 (2), 1499-1511.https://doi.org/10.1039/D4TA07434C
62. Z. T. Xie; H. Wang; Y. Geng; M. Li; Q. Y. Deng; Y. Tian; R. Chen; X. Zhu; Q. Liao, "Carbon-Based Photothermal Superhydrophobic Materials with Hierarchical Structure Enhances the Anti-Icing and Photothermal Deicing Properties," *ACS Applied Materials & Interfaces* **2021,** 13 (40), 48308-48321.https://doi.org/10.1021/acsami.1c15028
63. W. Huang; J. X. Huang; Z. G. Guo; W. M. Liu, "Icephobic/Anti-Icing Properties of Superhydrophobic Surfaces," *Advances in Colloid and Interface Science* **2022,** 304.https://doi.org/10.1016/j.cis.2022.102658
64. W. L. Zhou; T. Wu; Y. Du; X. H. Zhang; X. C. Chen; J. B. Li; H. Xie; J. P. Qu, "Efficient Fabrication of Desert Beetle-Inspired Micro/Nano-Structures on Polypropylene/Graphene Surface with Hybrid Wettability, Chemical Tolerance, and Passive Anti-Icing for Quantitative Fog Harvesting," *Chemical Engineering Journal* **2023,** 453.https://doi.org/10.1016/j.cej.2022.139784
65. J. Yang; J. Li; P. Xu; B. Chen, "Robust and Transparent Superoleophobic Coatings from One-Step Spraying of SiO2@fluoroPOS," *Journal of Sol-Gel Science and Technology* **2020,** 93 (1), 79-90.https://doi.org/10.1007/s10971-019-05166-1